Inorganic Chemistry

Article

pubs.acs.org/IC

Layered Compounds $BaM_2Ge_4Ch_6$ (M = Rh, Ir and Ch = S, Se) with Pyrite-Type Building Blocks and Ge−Ch Heteromolecule-Like Anions

Hechang Lei,[†] Jun-ichi Yamaura,[‡] Jiangang Guo,[†] Yanpeng Qi,[†] Yoshitake Toda,[†] and Hideo Hosono*[,†,‡,§]

[†]Frontier Research Center, Tokyo Institute of Technology, Yokohama 226-8503, Japan

[‡]Materials Research Center for Element Strategy, Tokyo Institute of Technology, Yokohama 226-8503, Japan

[§]Materials and Structures Laboratory, Tokyo Institute of Technology, Yokohama 226-8503, Japan

Supporting Information

ABSTRACT: The structures and chemical features of layered compounds $BaM_2Ge_4Ch_6$ (M = Rh, Ir; Ch = S, Se) synthesized by high-pressure and high-temperature methods have been systematically studied. These compounds crystallize in an orthorhombic phase with space group *Pbca* (No. 61). These compounds have the remarkable structural feature of M−Ge−Ch pyrite-type building units, stacking with Ba−Ch layers alternatively along the *c* axis. It is very rare and novel that pyrite-type subunits are the building blocks in layered compounds. Theoretical calculations and experimental results indicate that there are strongly polarized covalent bonds between Ge and Ch atoms, forming heteromolecule-like anions in these compounds. Moreover, Ge atoms in this structure exhibit an unusual valence state (∼+1) due to the tetrahedral coordination environment of Ge atoms along with M and Ch atoms simultaneously.

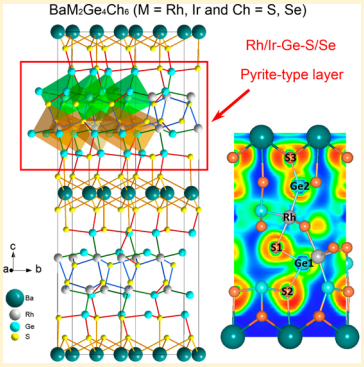

INTRODUCTION

Hundreds of inorganic compounds with MCh_2, MX'_2, or MChX′ formulas (M = post transition metals, Ch = chalcogens, and X′ = tetrels or pnictogens) have a pyrite-type structure, which originates from FeS_2 and is the most common structure of the sulfide minerals. The structure is composed of a three-dimensional network of corner-sharing M-centered octahedra with Ch and/or X′ atoms at the vertices. The most remarkable feature is the bonding state between two Ch (X′) atoms, such as the S−S bond in FeS_2. The valence state and strength of this molecule-like anion (dimer) can change with different bond lengths of the dimer and can also be influenced by the position of the d(e_g) level of the transition metal relative to the π^* orbital of the dimer.[1] This kind of variation of anionic dimer has important effects on the physical properties of pyrite-type compounds. For example, in $NiS_{2-x}Se_x$, there is a metal−insulator transition with increasing *x* and the bonding−antibonding splitting in the S−S (Se−Se) dimer is identified as the main parameter controlling the size of the charge gap.[2,3] On the other hand, the Ir filling in pyrite-type Ir_xSe_2 probably enables the control of superconductivity because the electronic state is closely related to the distance of the Se−Se dimer.[4] Moreover, in $Ir_{0.94-x}Rh_xSe_2$, when the Se−Se dimer becomes destabilized (weakened) accompanied by partial electron transfer from the Ir/Rh to the Se, there is an enhanced superconducting T_c value in this system.[5]

In many Ge−Ch compounds, owing to the chemical similarity between Ge and Si as well as between O and Ch, a Ge atom tends to be coordinated by four Ch atoms to form the Ge−Ch tetrahedron $GeCh_4$, such as Eu_2GeS_4,[6] $PdGeS_3$,[7] Mn_2GeSe_4,[8] and $La_3CuGeSe_7$.[9] This building block is also an important structural unit in chalcogenide glasses, such as in binary $GeCh_2$[10] and ternary GeS_2−SbS_3 as well as Ga_2Se_3−$GeSe_2$ systems.[11,12] In the Ge−Ch tetrahedron, Ge usually exhibits a positive valence state (+4) in the polarized covalent bond between Ge and Ch.

For ternary pyrite-type compounds, the compounds including Ge and Ch atoms simultaneously are scarce, and only two compounds, PtGeS and PtGeSe, have been reported until now.[13] They have a cobaltite structure, a ternary variant of the pyrite-type structure.[13] Although in these compounds Ge atoms are located at the center of the tetrahedron, similar to the case for other Ge−Ch compounds, atoms at the vertices of the tetrahedron are not only Ch but also Pt. In our search for new quaternary Ge−S/Se compounds, a new family of layered compounds $BaM_2Ge_4Ch_6$ (M = Rh, Ir; Ch = S, Se) with pyrite-type building units has been discovered. This structure is built up by stacking of M−Ge−Ch pyrite-type slabs and Ba−Ch layers alternately along the *c* axis. This is the first case where pyrite-type subunits have been utilized to build compounds with a complex structure. More importantly, theoretical calculations and experimental results indicate that there is a strong polarized covalent bond (dimer) between the Ge and Ch atoms. Moreover, the tetrahedral coordination of the Ge atom by both M and Ch atoms results in an unusually small

Received: February 26, 2014
Published: May 9, 2014

   dx.doi.org/10.1021/ic500437k | *Inorg. Chem.* 2014, 53, 5684−5691

positive valence state of Ge (~+1) in these compounds, which is significantly different from the valence state of Ge (+4) in other Ge−Ch compounds with only the Ge−Ch tetrahedron. This can be ascribed to the different electronegativities of Rh, Ge, and Ch atoms and the special coordination environment of the Ge atom.

EXPERIMENTAL SECTION

Synthesis. Polycrystalline $BaM_2Ge_4Ch_6$ compounds were synthesized using high-pressure and high-temperature methods. First, the BaS/BaSe precursors were prepared by sealing Ba and S/Se into silica tubes and sintering at 1073 K for 15 h. The obtained materials were mixed with stoichiometric amounts of Rh/Ir, Ge, and S/Se, ground well, and then pelletized. The pellet was loaded into an *h*-BN capsule and then heated to 1473 K and 5 GPa for 2 h using a belt-type high-pressure apparatus. All starting materials and precursors for the synthesis were prepared in a glovebox filled with purified Ar gas (H_2O, O_2 <1 ppm). Single crystals of $BaRh_2Ge_4S_6$ with a typical size of up to 0.05 × 0.05 × 0.01 mm were grown by prolonging the annealing time (12 h) under high pressure.

X-ray Powder Diffaction and Elemental Analysis. The powder X-ray diffraction (PXRD) patterns of $BaM_2Ge_4Ch_6$-filled capillary tubes were collected by using a Bruker D8 ADVANCE diffractometer with Mo Kα radiation (see the Supporting Information). Rietveld refinement of the XRD patterns was performed using the code TOPAS4.[14] The chemical compositions of the samples were examined by electron probe microscope analysis (EPMA) in the backscattered electron (BSE) mode. Sample analysis confirmed the presence of only Ba, Rh/Ir, Ge, and S/Se.

Structural Determination. Single-crystal X-ray diffraction experiments were carried out on a curved imaging plate (Rigaku R-AXIS RAPID-II) using Mo Kα radiation generated by a rotating anode with a confocal mirror (Rigaku VariMax). Data integration and absorption correction were performed with RAPID-AUTO. The charge-flipping method was used to decide the initial structural parameters.[15] Structural parameters were refined using the program SHELXL on the basis of the full-matrix least-squares method.[16] Anisotropic displacement parameters were applied for all atoms.

XPS Spectroscopy. X-ray photoelectron spectroscopy (XPS) measurements were performed using a hemispherical analyzer (Omicron, EA125) with nonmonochromatic X-ray (Al Kα line, $h\nu$ = 1486.7 eV, ΔE = 1.0 eV) sources. Samples were placed in an ultrahigh-vacuum apparatus with a base pressure of 2 × 10^{-8} Pa. The energy scale of XPS spectra was calibrated to the Au $4f_{7/2}$ peak at 84.0 eV.

Theoretical Calculations. First-principles electronic-structure calculations were performed using experimental crystallographic parameters within the full-potential linearized augmented-plane-wave (FP-LAPW) method implemented in the WIEN2k package.[17,18] The general gradient approximation (GGA) proposed by Perdew et al. was used for exchange-correlation potential.[19] The product of the muffin-tin radius (R_{MT}) and the largest wavenumber of the basis set (K_{max}) was fixed at 7.0 for all of calculations. We employed the following R_{MT}: $R_{MT\text{-}Ba}$ = 2.5 Bohr for all of four compounds, $R_{MT\text{-}Rh}$ = 2.29/2.30 Bohr for $BaRh_2Ge_4S_6/BaRh_2Ge_4Se_6$, $R_{MT\text{-}Ir}$ = 2.37/2.32 bohr for $BaIr_2Ge_4S_6/BaIr_2Ge_4Se_6$, $R_{MT\text{-}Ge}$ = 2.18/2.19/2.14/2.10 bohr for $BaRh_2Ge_4S_6/BaRh_2Ge_4Se_6/BaIr_2Ge_4S_6/BaIr_2Ge_4Se_6$, $R_{MT\text{-}S}$ = 1.92/1.85 bohr for $BaRh_2Ge_4S_6/BaIr_2Ge_4S_6$, and $R_{MT\text{-}Se}$ = 2.19/2.23 bohr for $BaRh_2Ge_4Se_6/BaIr_2Ge_4Se_6$, respectively. Self-consistency was carried out on 8 × 8 × 12 *k*-point meshes in the whole Brillouin zone. The energy convergence was set to be 10^{-4} Ry for self-consistency. Additionally, electronic structure calculations and bonding analyses were carried out for $BaRh_2Ge_4S_6$ using the tight binding−linear muffin -in orbitals−atomic sphere approximation (TB-LMTO-ASA) program package.[20] Radii of the atomic spheres and interstitial empty spheres were determined by the procedures implemented in the TB-LMTO-ASA programs. The *k*-space integration was performed by the tetrahedron method.[21] The Barth−Hedin exchange potential was employed for LDA calculations.[22] The radial scalar-relativistic Dirac equation was solved to obtain the partial waves. A basis set containing Ba(6s,5d,4f), Rh(5s,5p,4d), Ge(4s,4p), and S(3s,3p) orbitals was employed for a self-consistent calculation with Ba(6p), Rh(4f), Ge(4d), and S(3d) functions being down-folded, as automatically selected by the TB-LMTO-ASA program. For bonding analysis, the energy contributions of all electronic states for selected atom pairs were evaluated with a crystal orbital Hamiltonian population (COHP) analysis.[23] Integration up to the Fermi level yielded -ICOHP values as measures of relative overlap populations. The electron localization function (ELF)[24−26] was evaluated with modules implemented within the TB-LMTO-ASA program package. The VESTA program was used for visualization of ELF isosurfaces.[27]

RESULTS AND DISCUSSION

Structural Description. According to single-crystal X-ray diffraction analyses, $BaRh_2Ge_4S_6$ is a layered compound, which can be described well using the orthorhombic space group *Pbca* (No. 61) ($a \approx 5.95$ Å, $b \approx 5.89$ Å, $c \approx 29.20$ Å, and $Z = 4$) with seven independent atom sites (Tables 1 and 2). As shown in Figure 1a, this structure contains two building units stacking alternately along the *c* axis: (1) Ba−S layers and (2) Rh−Ge/S slabs. For the former unit, 1 Ba atom is surrounded by 10 S atoms, and the formed Ba−S2/S3 dodecahedra connect each other with face sharing and expand along the *ab* plane (Figure 1b). The bond lengths between Ba and S2/S3, $d_{Ba-S2/S3}$, spread out in the range between 3.229 and 3.361 Å (Table S1 of the Supporting Information), essentially corresponding to the sum of ionic radii. This indicates that the Ba−S bond type should be ionic. Moreover, these bond lengths are slightly larger than those in BaS at ambient ($d_{Ba-S} \approx 3.194$ Å, 6-coordination) and high pressure ($d_{Ba-S} \approx 3.159$ Å, 8-coordination) but are comparable to the values in BaS_3 ($d_{Ba-S} \approx 3.204-3.541$ Å, 12-coordination).[28,29] This could be partially ascribed to the rather high coordination number (10) of Ba in $BaRh_2Ge_4S_6$, which increases the steric effects.

On the other hand, the apparent complexities of this structure arise from the Rh−Ge/S slabs. First, there are two layers of Rh atoms and in each layer Rh atoms form a distorted square net (Figure S1 in the Supporting Information). The relative displacement of the second layer to the first layer is about (0, 0.5*b*, 0.1*c*). It should be noted that the interlayer distances of Rh atoms are slightly smaller than intralayer

Table 1. Crystal Data and Structure Refinement Details for $BaRh_2Ge_4S_6$

formula	$BaRh_2Ge_4S_6$
formula wt	826.09
radiation	Mo Kα
cryst syst	orthorhombic
space group	*Pbca* (No. 61)
Z	4
a (Å)	5.9512(1)
b (Å)	5.8941(1)
c (Å)	29.2011(5)
V (Å^3)	1024.30(3)
calcd density (g cm^{-3})	5.36
abs coeff (mm^{-1})	19.7
no. of rflns collected/R_{int}	12779/0.020
no. of data/params	3836/62
GOF	1.034
R1/wR2 ($I > 2\sigma(I)$)	0.024/0.045
extinction coeff	0.0007
largest diff peak/hole (e Å^{-3})	1.29/1.82

dx.doi.org/10.1021/ic500437k | Inorg. Chem. 2014, 53, 5684−5691

Table 2. Atomic Coordinates and Equivalent Isotropic Displacement Parameters for $BaRh_2Ge_4S_6$

atom	Wyckoff	*x*	*y*	*z*	U_{eq}[a] (10^3 Å^2)
Ba	4*a*	0	0	0	10.33(3)
Rh	8*c*	0.00302(2)	0.50948(2)	0.200697(5)	4.07(3)
Ge1	8*c*	0.37941(3)	0.38733(3)	0.184156(7)	5.60(4)
Ge2	8*c*	0.08079(3)	0.91701(4)	0.376698(7)	7.02(4)
S1	8*c*	0.11946(7)	0.62410(7)	0.27672(2)	5.15(7)
S2	8*c*	0.03560(8)	0.50918(8)	0.38690(2)	7.22(7)
S3	8*c*	0.00525(8)	0.49642(8)	0.05140(2)	9.25(8)

[a] U_{eq} is the equivalent isotropic displacement factor, defined as one-third of the trace of the orthogonalized U_{ij} tensor.

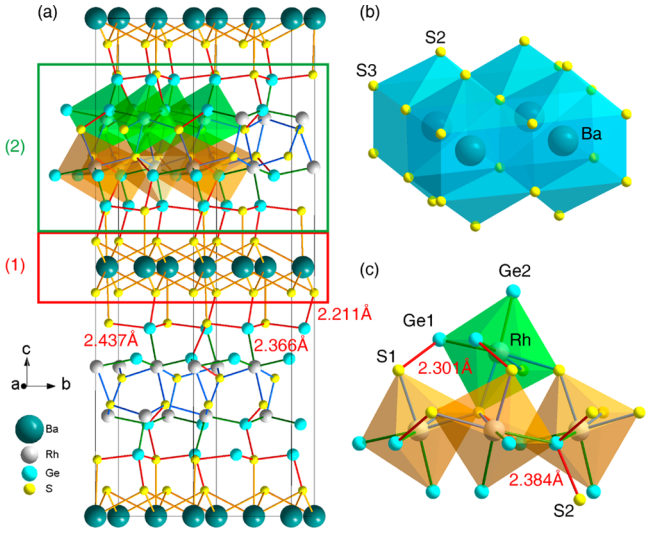

Figure 1. (a) Structure of $BaRh_2Ge_4S_6$. The octahedron of Rh−Ge/S is emphasized. The atoms are marked as follows: Ba, dark cyan; Rh, white; Ge, light blue; S, yellow. The building blocks (1) and (2) (see text) are emphasized by red and green rectangles. (b) View of a section of the Ba−S layer. Ba is located in the dodecahedron of S. (c) View of part of the Rh−Ge/S layer. The Ge−S bonds are labeled in red, and the corresponding bond lengths are shown.

distances. One Rh atom is coordinated with three Ge atoms (2 × Ge1 and 1 × Ge2) and three S atoms (3 × S1), forming one Rh−Ge/S octahedron (Figure 1c). In the Rh−Ge/S octahedron, Ge and S are ordered in a facial arrangement. Because of distinct bond lengths for all Rh−Ge/S bonds, especially for Rh−Ge and Rh−S (Table S1 in the Supporting Information), the Rh−Ge/S octahedra are highly distorted. This is also proved by the scattered bond angles of Ge/S−Rh−Ge/S deviating from the ideal values (90° or 180°) (Table S1 in the Supporting Information). The Rh−S bond lengths are between 2.422 and 2.475 Å, assuming that the valence of Rh is +3, the ionic radius of Rh^{3+} is 0.805 Å, and the bond lengths between Rh and S are close to the sum of ionic radii (2.505 Å), implying that the chemical bond of Rh−S should be ionic. However, the following detailed analysis indicates that there are strongly polarized covalent bonds rather than pure ionic bonds existing between Rh and S atoms. The distorted Rh−Ge/S octahedra are connected to each other by corner sharing, forming an extended two-dimensional (2D) network along the *ab* plane (Figure 1c).

On the other hand, S1 and Ge1/Ge2 have tetrahedral coordination (Figure 1c). S1 is shared by three Rh−Ge/S octahedra, and the fourth bond connects to Ge1. Ge1 bridges two Rh−Ge/S octahedra and connects with two sulfur atoms. One (S1) is between the Rh layers and another (S2) is out of the Rh−Ge/S slabs. In contrast, Ge2 only connects one Rh−Ge/S octahedron and the other three bonds connect with three sulfur atoms (2 × S2 and 1 × S3). The bond lengths between Ge and S atoms d_{Ge-S} are in the range 2.211−2.437 Å, and the Ge2−S3 bond length is the shortest among Ge−S bonds. Providing that the valences of Ba, Rh, and S are +2, +3 and −2, respectively, we obtain a +1 valence for Ge. For the S^{2-} anion and Ge^{2+} cation, the ionic radii are 1.70 and 0.87 Å, respectively; thus, the bond lengths between Ge and S are significantly smaller than the sum of ionic radii of S^{2-} and Ge^{2+} (2.57 Å), let alone the sum of ionic radii of S^{2-} and Ge^{+}. This clearly indicates that there are strong bonding interactions between Ge and S atoms, suggesting that the bonding type might be not purely ionic but rather polarized covalent.

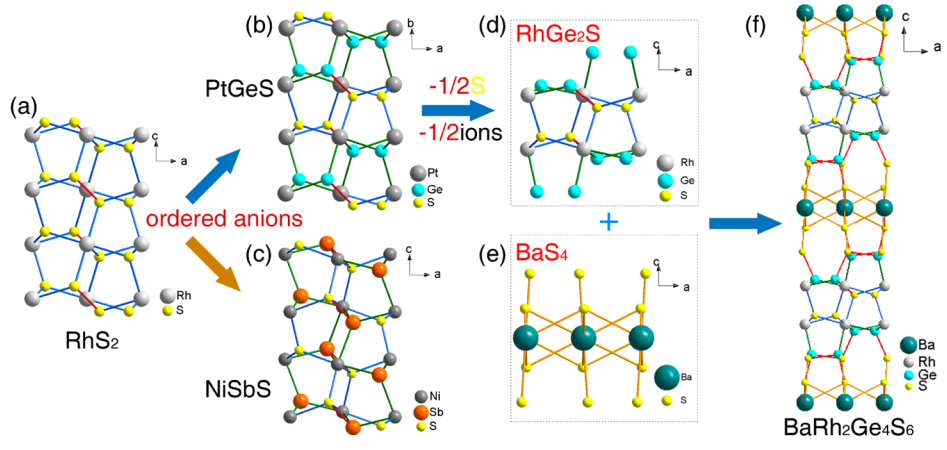

Figure 2. Structures of (a) RhS_2, (b) PtGeS, (c) NiSbS, (d) $RhGe_2S$ subunit, (e) BaS_4 subunit, and (f) $BaRh_2Ge_4S_6$.

dx.doi.org/10.1021/ic500437k | Inorg. Chem. 2014, 53, 5684−5691

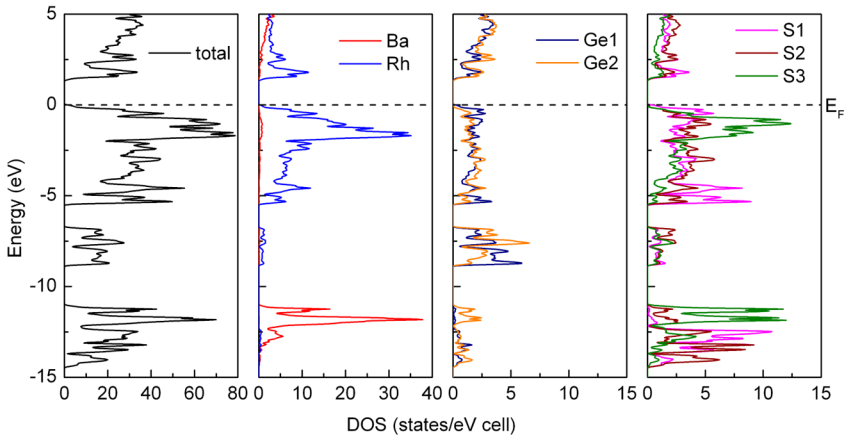

Figure 3. Calculated total DOS and PDOS for $BaRh_2Ge_4S_6$. A horizontal dashed line marks the Fermi level E_F, which has been arbitrarily set to 0 throughout this work. It should be noted that the ranges are different for the total DOS and PDOS.

Relation to Pyrite-Type Structure. At first, a layered $BaRh_2Ge_4S_6$-type structure seems to be an isolated new structure. In fact, it is closely related to the famous pyrite-type structure. Figure 2a shows the structure of the pyrite-type compound RhS_2. When half of the S atoms are replaced by other atoms, such as tetrels or pnictogens, they can form different ordered ternary pyrite-type compounds, known as the cobaltite-type (CoAsS) (Figure 2b) and the ullmannite-type (NiSbS) structures (Figure 2c).[30] PtGeS has the cobaltite-type structure (Figure 2b). If Pt is replaced by Rh and half of the Rh and S atoms are removed, an $RhGe_2S$ subunit will be obtained (Figure 2d). In combination with the BaS_4 subunit (Figure 2e), we finally get the $BaRh_2Ge_4S_6$ structure (Figure 2f). Therefore, the newly synthesized $BaRh_2Ge_4S_6$ may be regarded to have an intergrowth structure of ternary pyrite-type slabs and Ba−S layers along the *c* axis. As far as we know, this is the first layered structure containing a pyrite-type subunit. It may be possible to discover more potential homologous series of layered compounds in this family, like other well-known families such as the Ruddlesden−Popper series and Sillén−Aurivillius series.

Electronic Structure Calculations. In order to understand the physical properties and chemical bonding of $BaRh_2Ge_4S_6$, first-principles and TB-LMTO calculations were carried out. Figure 3 shows the total and partial densities of states (DOS and PDOS) for the $BaRh_2Ge_4S_6$ calculated by the DFT method. The Fermi energy level (E_F, set as 0) is located at the edge of the valence band, indicating that $BaRh_2Ge_4S_6$ is a semiconductor with the band gap E_g = 1.389 eV. There are three separate sets of bands in the valence region. The lowest region, ranging from −14.5 to −11 eV (relative to E_F), contains mainly the Ba 5p and S 3s states with a small mixture of the Ge 4s state. The second region from −9 to −6.6 eV is principally composed of the Ge 4s state with some mixture of S 3s and S 3p states. The third region starting from −5.6 eV and going up to E_F is dominated by Rh 4d, S 3p, and Ge 4p states. Above the E_F value, the unoccupied states originate mostly from the Rh 3d, S 3p, Ge 4s/4p, and Ba 5d states. As shown in Figure 3, the PDOS weights of Ge and S atoms at the valence band and the conduction band near E_F are similar, suggesting that Ge and S atoms are not purely ionic and should have significantly covalent interactions with neighboring atoms to some extent. This has been confirmed by the following bonding analysis.

Chemical Bonding. Because the type and strength of chemical bonds between two Ch (X′) elements are crucial in pyrite-type compounds, the chemical bonds in $BaRh_2Ge_4S_6$, especially between Ge and S atoms, need to be clarified. In order to obtain a quantitative measure of the bond strength, the crystal orbital Hamiltonian populations (−COHPs) and integrated COHP values (-ICOHPs) up to E_F of select interatomic contacts have been calculated (Figure 4 and Table 3). From Figure 4a, it can be seen that the Rh−Ge1(2) bonds are optimized with all bonding states below the Fermi level and anitbonding states above the Fermi level. However, the Rh−S1 bonds have mainly been optimized with small antibonding contributions around the Fermi level (Figure 4b). Similar to the case for Rh−Ge/S bonds, Ge−S bonds exhibit mainly bonding states below E_F with slightly antibonding states between −8 and −7 eV (Figure 4c,d). It should be noted that there is a strong

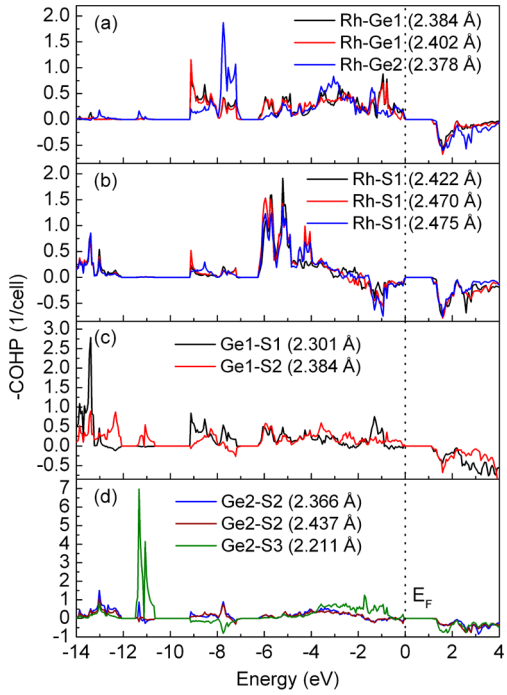

Figure 4. Calculated COHPs of (a) Rh−Ge1(2), (b) Rh−S1, (c) Ge1−S1(2), and (d) Ge2−S2(3) interactions. The distances of each atomic pair are given in brackets. A vertical dashed line marks the Fermi level E_F.

dx.doi.org/10.1021/ic500437k | Inorg. Chem. 2014, 53, 5684−5691

Table 3. Selected Bond Lengths and Corresponding -ICOHP Values for $BaRh_2Ge_4S_6$

bond	distance (Å)	-ICOHP (eV/cell)	bond	distance (Å)	-ICOHP (eV/cell)
Ba−S2	3.3099(5)	0.12	Rh−S1	2.4218(5)	2.05
Ba−S3	3.2886(5)	0.35	Rh−S1	2.4701(4)	2.12
Ba−S3	3.3049(5)	0.29	Rh−S1	2.4750(5)	1.89
Ba−S3	3.3262(5)	0.27	Ge1−S1	2.3008(5)	2.70
Ba−S3	3.3607(5)	0.32	Ge1−S2	2.3844(5)	2.35
Rh−Ge1	2.3839(2)	2.53	Ge2−S2	2.3655(5)	2.18
Rh−Ge1	2.4019(2)	2.43	Ge2−S2	2.4371(5)	1.81
Rh−Ge2	2.3777(2)	2.67	Ge2−S3	2.2113(5)	3.83

bonding state at about −11 eV for the Ge2−S3 contact, which originates from the strong interaction between Ge2 4s and S3 3s states. This strong interaction also leads to the largest -ICOHP value (3.83 eV/cell) for Ge2−S3 among all the interatomic contacts (Table 3). Moreover, it can be seen that the -ICOHP values are roughly inversely proportional to bond lengths: i.e., the larger -ICOHP values correspond to shorter bonds and possibly stronger interactions. In addition to the strongest Ge2−S3 bonding state, the second highest -ICOHP value is found for the Ge1−S1 bond, indicating the remarkable trend of bonding between Ge and S atoms in the pyrite-type slab. On the other hand, the -ICOHP values for Rh−Ge1(2) and Rh−S1 are comparable to those of Ge−S bonds, indicating that there are also strong bonding interactions between Rh and Ge/S. In contrast, the small -ICOHP values (≤0.35) for the Ba−S2(3) bond reflect the weak interaction between Ba and S2(3).

Further insight into the nature of the chemical bonding in $BaRh_2Ge_4S_6$ is provided by an electron localization function (ELF) analysis, as shown in Figure 5. The ELF maxima in the region of the valence electrons indicate either covalent bonds or lone electron pairs. The attractors ① and ② correspond to Rh−Ge1/2 interactions. The ELF maxima are located between Rh−Ge connecting lines, which is typical for the two-center bonds. However, they are obviously shifted toward Ge atoms, meaning that the Rh−Ge1/2 bonds are remarkably polarized and there is significant charge transfer from Rh to Ge1/2. This charge transfer suggests that the Allred−Rochow electronegativity scale could be more suitable for this compound than the Pauling electronegativity scale because the Pauling electronegativity of Ge (2.01) is slightly smaller than that of Rh (2.28) leading to the charge transfer from Ge to Rh.[31−33] On the other hand, the Allred−Rochow electronegativity of Ge (2.02) is larger than that of Rh (1.45);[34,35] thus, it gives the correct polarity of Rh−Ge bonds. Covalent bonding also occurs between Rh and S1 atoms (③) with even stronger polarity.

For Ge−S bonding, the localization domains between Ge and S atoms (④−⑦) also shift away from the center of Ge−S connecting lines and are polarized around the S atoms. However, this trend is weaker than that in Rh−Ge/S bonds because of the smaller difference of electronegativity between Ge (2.02) and S (2.44). Therefore, the type of chemical bonding between Ge1 and S1 atoms in a pyrite-type slab is a polarized covalent bond. This clearly shows that there are heteromolecule-like anions (dimers) composed of Ge and S atoms, which interact with cation-like Rh atoms. Moreover, the

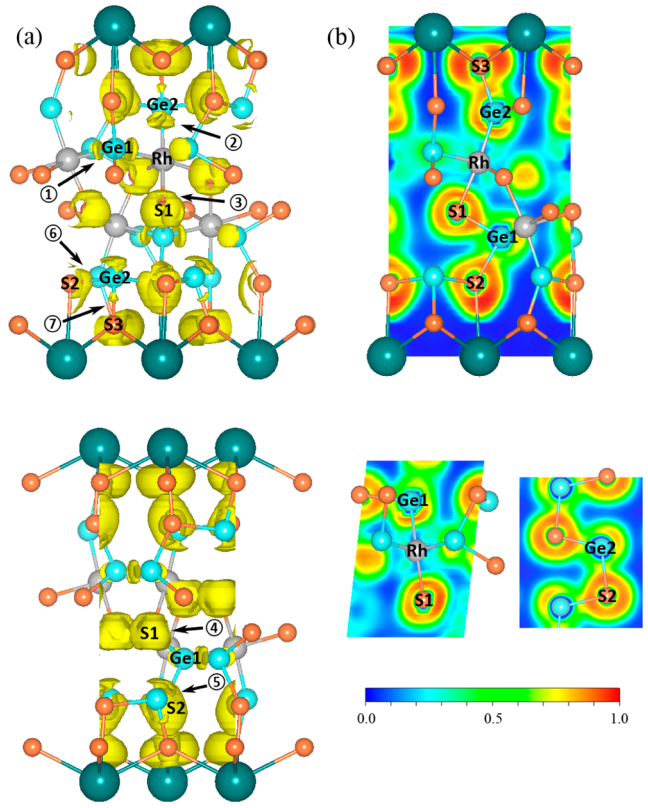

Figure 5. (a) 3D isosurfaces of the electron localization function (ELF, η) for $BaRh_2Ge_4S_6$ (η = 0.8). (b) 2D ELF contour plots for slices of the crystal structure of $BaRh_2Ge_4S_6$.

unique tetrahedral coordination environment of Ge atoms and the different electronegativities of Rh, Ge, and S lead to the unusual valence state of Ge in this compound, as discussed below.

On the other hand, the lone electron pairs of S2 and S3 atoms near Ba atoms are clearly shown in Figure 5b. However, the shape of lone electron pairs for the S3 atom is different from that for S2 because of different coordination environments. The former has a nearly spherical-like shape due to four Ba atoms surrounding the bottom part of S3; in contrast, the latter has an ellipsoidal shape. In addition, for S3 atoms, such high density of the lone electron pair pushes the valence electron toward the Ge2 side, resulting in the weakening of polarity of localization domains and the strongest interaction (shortest bond length) for the Ge2−S3 contact in comparison to bonds (Figure 5b). This could explain the huge peak in Figure 4d at about −11 eV for the Ge2−S3 contact.

XPS Spectra. In order to confirm above theoretical analysis, the valence states of Ba, Rh, Ge, and S in $BaRh_2Ge_4S_6$ were investigated using XPS. Figure 6a shows the XPS spectrum of Ba $3d_{5/2}$. The binding energy of Ba $3d_{5/2}$ is 779.5 eV, which is very close to that in BaS (779.8 eV).[36] This indicates that the valence state of Ba should be close to +2. For the XPS spectrum of Rh (Figure 6b), there are two peaks at 311.95 and 307.45 eV, corresponding to Rh $3d_{3/2}$ and $3d_{5/2}$, respectively. In comparison to Rh_2O_3 (309.1 eV) and Rh_2S_3 (308.6 eV),[37,38] the peak position of Rh $3d_{5/2}$ in $BaRh_2Ge_4S_6$ is shifted to lower binding energy, implying that the valence state of Rh is smaller than +3. Because the Rh−Ge/S bonds are not purely ionic but polarized covalent and the electronegativity of Ge is smaller than that of S, both factors might lead to the valence of Rh

dx.doi.org/10.1021/ic500437k | Inorg. Chem. 2014, 53, 5684−5691

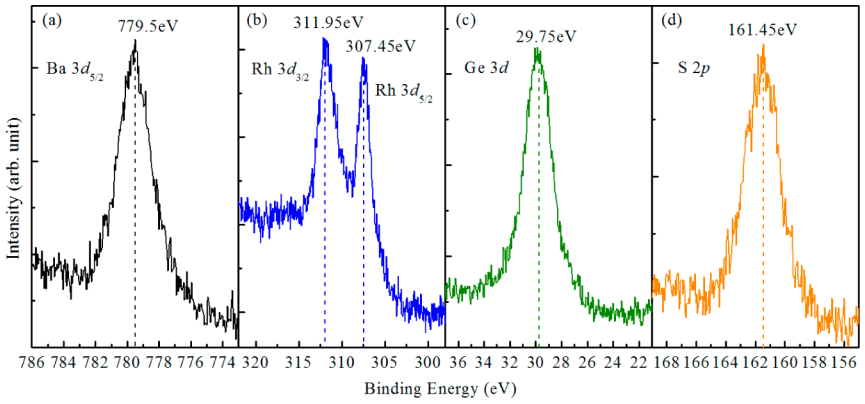

Figure 6. XPS spectra of (a) Ba 3d, (b) Rh 3d, (c) Ge 3d, and (d) S 2p in $BaRh_2Ge_4S_6$.

being smaller than +3. This is consistent with the theoretical analysis. For the XPS spectrum of Ge, the binding energy of Ge 3d is about 29.75 eV (Figure 6c), which is significantly smaller than 32.5 eV corresponding to the Ge^{4+} in GeO_2.[39] This means that the valence state of Ge is much lower than +4. The binding energy is even smaller than those in GeS (30.5 eV) and GeSe (30.9 eV).[40] On the other hand, this value is larger than that of elemental Ge (29.0 eV),[40] clearly indicating that the valence of Ge in $BaRh_2Ge_4S_6$ is positive. Schmeisser et al. proposed that an average chemical shift per oxidation state for Ge 3d core level is 0.85 eV.[41] If 29.0 eV is taken as the binding energy for the elemental Ge 3d core level,[40] the binding energy of the Ge^+ 3d core level should be 29.85 eV, which is very close to the observed value. Thus, it confirms that the valence state of Ge should be close to +1 in $BaRh_2Ge_4S_6$. The small positive valence state of Ge can be understood as follows. Ge atoms are anionic-like in Rh−Ge bonds; thus, it should exhibit a negative valence state. However, this is compensated by the positive valence state of Ge atoms in Ge−S bonds and finally has a small positive valence state that is still smaller than that in GeS. For the XPS spectrum of S 2p (Figure 6d), the spectral peak position (161.45 eV) is similar to that in TiS_2 (161.5 eV).[42] This confirms that the valence state of S should be close to −2. On the other hand, the peak position shifts to lower energy in comparison to that of FeS_2 (162.4 eV), in which there are unpolarized S−S covalent bonds.[1,43] This is consistent with the theoretical results showing the strong polarity of Ge−S covalent bonds. According to the results of XPS spectra and theoretical calculations, if we assume that the valence state of Ba is +2, that of Rh is $+(3-\delta)$, and that of S is −2, the charge-balanced formula of $BaRh_2Ge_4S_6$ can be described as $(Ba^{2+})(Rh^{(3-\delta)+})_2(Ge^{+(1+\delta/2)})_4(S^{2-})_6$.

Isostructural Compounds. In order to extend the phase range of this novel structure type, we also tried to synthesize the compounds $(Ba/Sr)(Co/Rh/Ir)_2(Ge/Sn)_4(S/Se/Te)_6$. Among these trials, three other compounds that are isostructural with $BaRh_2Ge_4S_6$ were discovered: $Ba(Rh/Ir)_2Ge_4(S/Se)_6$. The PXRD patterns are shown in Figure S2 in the Supporting Information, and the fitted lattice parameters are given in Table 4. The replacement of Rh by Ir does not change the lattice parameters too much, which can be ascribed to the similar ionic/covalent radii between Rh and Ir. On the other hand, the selenides expand the unit cell along all of the crystallographic directions because of the much larger ionic/covalent radii of Se in comparison to those of S. Moreover, for $BaIr_2Ge_4S_6$, we can not obtain a pure phase under the current synthesis conditions and secondary phases always exist (Figure S2 in the Supporting Information). These results suggest that $BaIr_2Ge_4S_6$ may be at the boundary of the phase range for this structure.

Table 4. Cell Parameters and Reliability Factors Obtained from Powder XRD Patterns Using Rietveld Refinements of $BaRh_2Ge_4S_6$, $BaIr_2Ge_4S_6$, $BaRh_2Ge_4Se_6$, and $BaIr_2Ge_4Se_6$ (Space Group *Pbca*)

	$BaRh_2Ge_4S_6$	$BaRh_2Ge_4Se_6$	$BaIr_2Ge_4S_6$	$BaIr_2Ge_4Se_6$
formula wt	826.09	1107.46	1004.71	1286.08
a (Å)	5.9473(2)	6.1318(3)	5.9480(4)	6.1346(4)
b (Å)	5.8891(2)	6.0700(3)	5.9148(4)	6.0870(4)
c (Å)	29.1781(9)	30.3144(9)	29.152(2)	30.279(1)
V (Å^3)	1021.94(6)	1128.29(8)	1025.6(1)	1130.6(1)
R_p (%)	5.74	4.32	5.43	5.08
R_{wp} (%)	8.25	6.41	7.85	7.54
GOF	2.79	1.68	2.03	1.80

Three other isostructural compounds have similar band structures with different band gaps (Figures S3−S5 in the Supporting Information). The band gaps are 1.089, 1.539, and 1.332 eV for $BaRh_2Ge_4Se_6$, $BaIr_2Ge_4S_6$, and $BaIr_2Ge_4Se_6$, respectively. There is a trend that the band gap becomes smaller when S is replaced by Se but increases when Rh is substituted by Ir. This is partially due to the increase of energy dispersion from enhanced orbital overlap when the p states of the chalcogen atoms make contributions to both the valence band maximum and conduction band minimum, and the p states become more extended for Se than S.

Although other combinations do not form the compounds isostructural with $BaRh_2Ge_4S_6$, they form other compounds structurally related to $BaRh_2Ge_4S_6$. For example, when Ba was replaced by Sr in $BaRh_2Ge_4S_6$ or Ge is replaced by Sn in $BaIr_2Ge_4Se_6$, we obtained $RhGe_{1.5}S_{1.5}$ or $IrSn_{1.5}Se_{1.5}$, an anionic ordered ternary skutterudite compound (Figure 7a).[44,45] They have the same M−Ge(Sn)/S(Se) (M = Rh and Ir) octahedra with a facial arrangement of ordered anions and corner-shared connectiona between octahedra as in some ternary pyrite-type compounds. However, the cation M sublattice arranges into a distorted simple-cubic geometry, different from the face-centered-cubic (fcc) geometry in pyrite-type compounds. This results in two anionic−anionic dimers for each anion (Figure 7a), in contrast to one dimer in pyrite-type compounds (Figure 7c). On the other hand, when Se is replaced by Te in $BaIr_2Ge_4Se_6$, IrGeTe is obtained as the main phase, which is a novel phase isostructural with RhGeTe. It has an anionic ordered ternary α-$NiAs_2$-type (pararammelsbergite) structure

dx.doi.org/10.1021/ic500437k | Inorg. Chem. 2014, 53, 5684−5691

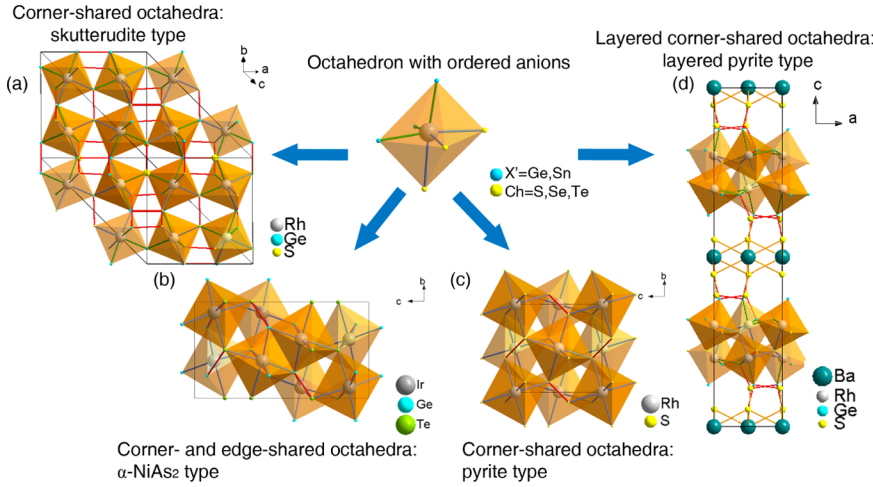

Figure 7. Different structures derived from M−Ch(X′) octahedra with ordered anions: (a) skutterudite type $RhGe_{1.5}S_{1.5}$; (b) α-$NiAs_2$ type IrGeTe; (c) pyrite-type RhS_2; (d) layered pyrite-type $BaRh_2Ge_4S_6$.

(Figure 7b).[46] M−Ge/Te octahedra with a facial arrangement of ordered anions also exist in this structure, similar to the case for pyrite-type compounds. However, half of the M sublattice with fcc geometry slides ∼0.28*b* along the *b* axis, leading to an edge-shared octahedral connection along the sliding plane (Figure 7b). The above results indicate that the basic units of M−Ch(X′) octahedra with ordered anions can construct different structures via different arrangements of units. There should be a competing relationship among these phases.

CONCLUSION

In summary, we have discovered the series of layered compounds $BaM_2Ge_4Ch_6$ (M = Rh, Ir; Ch = S, Se), which have been synthesized by high-pressure and high-temperature methods, and explored their chemical features systematically. A structural analysis reveals that these compounds contain unprecedented M−Ge−Ch pyrite-type layers. Theoretical calculations indicate that all of them are semiconductors. Experimental results combined with theoretical calculations further suggest that there are strongly polarized covalent bonds between Ge and Ch atoms, which have the largest electronegativity among Ba, M, Ge, and Ch. More interestingly, because of the special tetragonal coordination environment of Ge with M and Ch simultaneously and the different electronegativities of M, Ge, and Ch (M < Ge < Ch), Ge exhibits the unusual valence state ∼+1. As far as we know, this is the first series of layered compounds with pyrite-type building blocks. This indicates that a pyrite-type subunit can be used to build more complex compounds formed under certain nonequilibrium conditions, such as high pressure.

ASSOCIATED CONTENT

Supporting Information

Figures, a table, and a CIF file giving X-ray crystallographic data and selected bond distances and bond angles for $BaRh_2Ge_4S_6$, a powder XRD pattern and fitting results, and calculated total DOS/PDOS for $BaM_2Ge_4Ch_6$. This material is available free of charge via the Internet at http://pubs.acs.org.

AUTHOR INFORMATION

Corresponding Author

*E-mail for H.H.: hosono@msl.titech.ac.jp.

Notes

The authors declare no competing financial interest.

ACKNOWLEDGMENTS

This work was supported by the Funding Program for World-Leading Innovative R&D on Science and Technology (FIRST), Japan, and MEXT Elements Strategy Initiative to Form Core Research Center.

REFERENCES

(1) Jobic, S.; Brec, R.; Rouxel, J. *J. Alloys Compd.* **1992**, *178*, 253−283.
(2) Yao, X.; Honig, J. M.; Hogan, T.; Kannewurf, C.; Spałek, J. *Phys. Rev. B* **1996**, *54*, 17469−17475.
(3) Kuneš, J.; Baldassarre, L.; Schächner, B.; Rabia, K.; Kuntscher, C. A.; Korotin, Dm. M.; Anisimov, V. I.; McLeod, J. A.; Kurmaev, E. Z.; Moewes, A. *Phys. Rev. B* **2010**, *81*, 035122.
(4) Qi, Y. P.; Matsuishi, S.; Guo, J. G.; Mizoguchi, H.; Hosono, H. *Phys. Rev. Lett.* **2012**, *109*, 217002.
(5) Guo, J. G.; Qi, Y. P.; Matsuishi, S.; Hosono, H. *J. Am. Chem. Soc.* **2012**, *134*, 20001−20004.
(6) Tampier, M.; Johrendt, D. *J. Solid State Chem.* **2001**, *158*, 343−348.
(7) Tampier, M.; Johrendt, D. *Chem. Eur. J.* **1998**, *4*, 1829−1833.
(8) Deiseroth, H. J.; Aleksandrov, K. S.; Kremer, R. K. *Z. Anorg. Allg. Chem.* **2005**, *631*, 448−450.
(9) Poduska, K. M.; DiSalvo, F. J.; Min, K.; Halasyamani, P. S. *J. Alloys Compd.* **2002**, *335*, L5−L9.
(10) Elliott, S. R. *Nature* **1991**, *354*, 445−452.
(11) Golovchak, R.; Calvez, L.; Petracovschi, E.; Bureau, B.; Savytskii, D.; Jain, H. *Mater. Chem. Phys.* **2013**, *138*, 909−916.
(12) Lin, C.; Li, Z.; Ying, L.; Xu, Y.; Zhang, P.; Dai, S.; Xu, T.; Nie, Q. *J. Phys. Chem. C* **2012**, *116*, 5862−5867.
(13) Entner, P.; Parthé, E. *Acta Crystallogr., Sect. B* **1973**, *29*, 1557−1560.
(14) *TOPAS Version 4*; Bruker AXS, Karlsruhe, Germany, 2007.
(15) Palatinus, L.; Chapuis, G. *J. Appl. Crystallogr.* **2007**, *40*, 786−790.
(16) Sheldrick, G. M. *Acta Crystallogr., Sect. A* **2008**, *64*, 112−122.
(17) Blaha, P.; Schwarz, K.; Madsen, G. K. H.; Kvasnicka, D.; Luitz, J. *WIEN2k: An Augmented Plane Wave + Local Orbitals Program for Calculating Crystal Properties*; Technische Universität Wien, Wien, Austria, 2001.
(18) Schwarz, K. *J. Solid State Chem.* **2003**, *176*, 319−328.
(19) Perdew, J. P.; Burke, K.; Ernzerhof, M. *Phys. Rev. Lett.* **1996**, *77*, 3865−3868.

dx.doi.org/10.1021/ic500437k | *Inorg. Chem.* 2014, 53, 5684−5691

(20) Jepsen, O.; Burkhardt, A.; Andersen, O. K. *Program TB-LMTO-ASA, Version 4.7*; Max-Planck-Institut für Festkörperforschung, Stuttgart, Germany, 1999.
(21) Blöchel, P. E.; Jepsen, O.; Andersen, O. K. *Phys. Rev. B* **1994**, *49*, 16223−16233.
(22) von Barth, U.; Hedin, L. *J. Phys. C: Solid State Phys.* **1972**, *5*, 1629−1642.
(23) Dronskowski, R.; Blöchl, P. E. *J. Phys. Chem.* **1993**, *97*, 8617−8624.
(24) Becke, A. D.; Edgecombe, K. E. *J. Chem. Phys.* **1990**, *92*, 5397−5403.
(25) Savin, A.; Jepsen, O.; Flad, J.; Andersen, O. K.; Preuss, H.; von Schnering, H. G. *Angew. Chem., Int. Ed. Engl.* **1992**, *31*, 187−188.
(26) Savin, A.; Nesper, R.; Wengert, S.; Fassler, T. F. *Angew. Chem., Int. Ed. Engl.* **1997**, *36*, 1808−1832.
(27) Momma, K.; Izumi, F. *J. Appl. Crystallogr.* **2011**, *44*, 1272−1276.
(28) Yamaoka, S.; Shimomura, O.; Nakazawa, H.; Fukunaga, O. *Solid State Commun.* **1980**, *33*, 87−89.
(29) Yamaoka, S.; Lemley, J. T.; Jenks, J. M.; Steinfink, H. *Inorg. Chem.* **1975**, *14*, 129−131.
(30) Foecker, A. J.; Jeitschko, W. *J. Solid State Chem.* **2001**, *162*, 69−78.
(31) Pauling, L. *J. Am. Chem. Soc.* **1932**, *54*, 3570−3582.
(32) Allred, A. L. *J. Inorg. Nucl. Chem.* **1961**, *17*, 215−221.
(33) Dobrotin, R. B. *J. Struct. Chem.* **1963**, *4*, 810−813.
(34) Allred, A. L.; Rochow, E. G. *J. Inorg. Nucl. Chem.* **1958**, *5*, 264−268.
(35) Little, E. J., Jr.; Jones, M. M. *J. Chem. Educ.* **1960**, *37*, 231−233.
(36) Sinharoy, S.; Wolfe, A. L. *J. Electron Spectrosc. Relat. Phenom.* **1980**, *18*, 369−371.
(37) Contour, J. P.; Mouvier, G.; Hoogewijs, M.; Leclere, C. *J. Catal.* **1977**, *48*, 217−228.
(38) Givens, K. E.; Dillard, J. G. *J. Catal.* **1984**, *86*, 108−120.
(39) Barr, T. L.; Mohsenian, M.; Chen, L. M. *Appl. Surf. Sci.* **1991**, *51*, 71−87.
(40) Shalvoy, R. B.; Fisher, G. B.; Stiles, P. J. *Phys. Rev. B* **1977**, *15*, 1680−1697.
(41) Schmeisser, D.; Schnell, R. D.; Bogen, A.; Himpsel, F. J.; Rieger, D.; Landgren, G.; Morar, J. F. *Surf. Sci.* **1986**, *172*, 455−465.
(42) Siriwardane, R. V.; Poston, J. A. *Appl. Surf. Sci.* **1990**, *45*, 131−139.
(43) Volmer-Uebing, M.; Stratmann, M. *Appl. Surf. Sci.* **1992**, *55*, 19−35.
(44) Vaqueiro, P.; Sobany, G. G.; Stindl, M. *J. Solid State Chem.* **2008**, *181*, 768−776.
(45) Fleurial, J.-P.; Caillat, T.; Borshchevsky, A. *Proc. XVI Int. Conf. Thermoelec.* IEEE: Dresden, Germany, **1997**.
(46) Vaqueiro, P.; Sobany, G. G.; Guinet, F.; Leyva-Bailen, P. *Solid State Sci.* **2009**, *11*, 1077−1082.